

## Morphological and kinematic signatures of a binary central star in the planetary nebula Hu 2-1

Luis F. Miranda

*Instituto de Astrofísica de Andalucía, CSIC, Apdo. Correos 3004, E-18080 Granada, Spain.*

lfm@iaa.es

José M. Torrelles

*Institut d'Estudis Espacials de Catalunya (IEEC/CSIC) and Instituto de Ciencias del Espacio (CSIC), Edifici Nexus, C/ Gran Capitá 2-4, E-08034 Barcelona, Spain*

torrelles@ieec.fcr.es

Martín A. Guerrero

*Department of Astronomy, University of Illinois at Urbana-Champaign, 1002 West Green Street, Urbana, IL 61801 USA*

mar@astro.uiuc.edu

Roberto Vázquez

*Instituto de Astronomía, UNAM, Apto. Postal 877, 22800 Ensenada, B.C., Mexico*

vazquez@astrosen.unam.mx

Yolanda Gómez

*Instituto de Astronomía UNAM, Campus Morelia, A.P. 3-72 (Xangari), c.p. 58089 Morelia, Michoacán, Mexico*

gocy@astrosmo.unam.mx

### ABSTRACT

We present  $H\alpha$ , [NII] and [OIII] ground-based and HST archive images, VLA–A 3.6 cm continuum and  $H92\alpha$  emission line data and high resolution long-slit [NII] spectra of the planetary nebula Hu 2-1. A large number of structural components are identified in the nebula: an outer bipolar and an inner shell, two pairs of collimated bipolar structures at different directions, monopolar bow-shock-like structures and an extended

equatorial structure within a halo. The formation of Hu 2-1 appears dominated by anisotropic mass ejection during the late AGB stage of the progenitor and by variable, “precessing” collimated bipolar outflows during the proto-planetary nebula and/or early planetary nebula phases. Different observational results strongly support the existence of a binary central star in Hu 2-1, among them: (1) the observed point-symmetry of the bipolar lobes and inner shell, and the departures from axial symmetry of the bipolar lobes, (2) the off-center position of the central star, (3) the detection of mass ejection towards the equatorial plane, and (4) the presence of “precessing” collimated velocity of the bipolar shell. We propose that this velocity difference is a direct evidence of orbital motion of the ejection source in a binary system. From a deduced orbital velocity of  $\sim 10 \text{ km s}^{-1}$ , a semi-major axis of  $\sim 9\text{--}27 \text{ AU}$  and period of  $\sim 25\text{--}80 \text{ yr}$  are obtained, assuming a reasonable range of masses. These parameters are used to analyze the formation of Hu 2-1 within current scenarios of planetary nebula with binary central stars.

*Subject headings:* planetary nebulae: individual: (Hu 2-1) – ISM: kinematics and dynamics – ISM: jets and outflows – stars: mass loss

## 1. Introduction

Binary stars are emerging as a basic ingredient in the formation and evolution of many planetary nebulae (PNe). Binary scenarios, involving different kinds of systems, have been invoked to provide qualitative explanations for different observations including, among others, the common asphericity of the PN shells and the existence of collimated outflows in PNe (e.g. Morris 1987; Soker & Livio 1994; Soker 1996; Mastrodemos & Morris 1998, 1999). On the other hand, only a scarce number of wide (separation  $\sim 10^2\text{--}10^4 \text{ AU}$ , period  $\sim 10^3\text{--}10^6 \text{ yr}$ ) and close (separation  $\sim 1\text{--}35 R_{\odot}$ , period  $\sim 0.11\text{--}16 \text{ days}$ ) binary central stars are presently known (Ciardullo et al. 1999; Soker 1999; Bond 2000 and references therein), most likely because direct detection is severely hampered by the present instrumental resolution, the nature of the binary itself and/or of its (stellar or sub-stellar) companion, and even by the evolution of the system (i.e., the binary may not exist anymore, e.g., Soker 1996). Therefore, a reasonable alternative to infer the possible presence and properties of a binary central star is to search for the influence of binary evolution in the nebular properties (e.g. Soker 1998).

Hu 2-1 (PN G051.4+09.6) is a young PN whose properties suggest the existence of a binary central star. The main shell presents a bipolar morphology consisting of a bright equatorial toroid and two faint bipolar lobes (Aaquist & Kwok 1990; Kwok & Aaquist 1993, hereafter KA93; Miranda 1995, hereafter M95). An external ring-like structure, characterized by relatively high  $[\text{NII}]/\text{H}\alpha$  values, surrounds the bright toroid (M95). Two highly collimated, high-velocity bipolar knots have been detected along the main nebular axis ( $\text{PA} \simeq 320^\circ$ ) via high-resolution, long-slit spectroscopy

(M95). These knots present the typical properties of collimated outflows in PNe (e.g., Miranda 1999), although they also exhibit large differences in radial velocity and velocity width. Another collimated structure was also identified near the major nebular axis (M95). It shares some properties with the bipolar knots (small velocity dispersion, small size, strong [NII] emission) but it does not share the general inclination of the bipolar shell and the bipolar knots. On the basis of these observations, it has been suggested that a mass transferring binary central star could be involved in the formation of Hu 2-1 (M95). There are additional structural components in this complex PN. The 3.6 cm continuum map by KA93 reveals a small elliptical structure embedded in the toroid, suggesting that Hu 2-1 is a double shell PN, and a faint extended halo has been detected in long-slit spectra (M95). Moreover, irregular variations of 0.2–0.3 mag in UVB have been reported (Kostyakova 1992; Arkhipova et al. 1994). Acker et al. (1998) analyzed HIPPARCOS data and measured a proper motion for Hu 2-1 of  $\simeq 15 \times 10^{-3}$  arcsec yr $^{-1}$  towards PA  $\simeq 157^\circ$ . In addition, Acker et al. obtained a very small, unrealistic distance for Hu 2-1, which, according to the authors, could be due to influence of the nebula itself in the parallax measurement. We will therefore adopt here a distance of 2.35 kpc (see M95).

We have obtained different data on Hu 2-1 in order to study in more detail the different nebular components, testing the binary scenario. In this paper we present the results obtained.

## 2. Observations and Results

### 2.1. Optical imaging

Direct images of Hu 2-1 were obtained with the 2.56 m Nordic Optical Telescope (NOT)<sup>1</sup> at Roque de los Muchachos Observatory in 1996 August. The detector was a Tektronix 24 $\mu$ m CCD with 1024 $\times$ 1024 pixels. The scale in the focal plane is  $\simeq 0''.176$  pixel $^{-1}$ . The filters were: H $\alpha$  ( $\lambda_0 \simeq 6563$  Å, FWHM  $\simeq 9$  Å), [NII] ( $\lambda_0 \simeq 6584$  Å, FWHM  $\simeq 9$  Å) and [OIII] ( $\lambda_0 \simeq 5007$  Å, FWHM  $\simeq 30$  Å). Exposure time was 20 s in H $\alpha$ , 180 s in [NII] and 60 s in [OIII]. Seeing was  $\simeq 0''.72$  for the three images.

Figure 1 presents contour plots of the H $\alpha$ , [OIII] and [NII] images deduced from the ground-based data. Although the resolution of the ground-based images is lower than those of the HST (described below), we present the ground-based images because they are useful to compare with the long-slit spectra (§ 2.3) and to obtain a global view of the excitation conditions in the nebula (see below). By comparing the images with the spectra previously presented (M95), the different structures can be identified. These are labeled in the [NII] image. Structure A corresponds to the bright equatorial toroid. It appears elongated along the nebular minor axis (PA  $50^\circ$ ) in H $\alpha$  and [NII] but circular in [OIII]. The bipolar lobes correspond to structure B. C1–C2 are the compact

---

<sup>1</sup>The Nordic Optical Telescope is operated on the Island of La Palma by NOTSA in the Spanish Observatorio del Roque de los Muchachos of the Instituto de Astrofísica de Canarias.

knots along the nebular major axis. C3–C4 are two compact structures at PA  $\simeq 350^\circ$ , reported for the first time in this paper. Component D is revealed to be an elongated structure oriented almost perpendicular to the nebular major axis. The images confirm that no counterpart of D exists towards the NW (M95). The existence of the extended (size  $\simeq 14''$ ) halo is confirmed. Structures within the halo can be recognized near the North-South direction, almost coinciding with C3–C4, and along PA  $\simeq 80^\circ$ . In addition, a bright region within the halo is observed along the nebular minor axis up to  $\simeq 6''$  from the center.

In order to gain a better view of Hu 2-1 we have retrieved the WFPC2 H $\alpha$ , [NII] and PC [OIII] images obtained with the *Hubble Space Telescope* from the HST archive (program ID: 6347, PI: K.J. Borkowski & J.P. Harrington for the H $\alpha$  and [NII] images; program ID: 3603, PI: M. Bobrowski for the [OIII] image). Figure 2 shows grey scale maps of the [NII] image and Figure 3 presents a grey-scale map of the central nebular regions as deduced from the H $\alpha$  image. The HST images confirm the basic bipolar structure of the nebula deduced from long-slit observations (M95). The bright toroid resembles a cylinder. If we assume circular cross section, the axis of the toroid is tilted  $\simeq 37^\circ$  with respect to the plane of the sky, in excellent agreement with the inclination angle deduced from long-slit spectra (M95). A small structure within the toroid is also observed and corresponds to the inner elliptical shell identified by KA93. This inner shell is extremely faint in [NII] but very bright in H $\alpha$  and [OIII] (not shown here). The HST images show that this shell presents open ends (see also below). The bipolar lobes also present point-symmetry with respect to the central star but they are not symmetric with respect to the main nebular axis. In particular, if we consider PAs  $310^\circ$  and  $330^\circ$ , which are symmetric with respect to the main axis (PA  $320^\circ$ ), the lobes are more extended at PA  $330^\circ$ , radius  $\simeq 2''.2$ , than at PA  $310^\circ$ , radius  $\simeq 1''.9$ . Finally, an elongated faint structure, particularly bright in H $\alpha$ , is observed at PA  $\simeq 80^\circ$  and corresponds to that identified in the ground-based images.

The central star is clearly observed in the HST images (Figs.2 and 3). As a remarkable result, we find that its position does not coincide with the center of the toroid but it is slightly displaced towards the SW along the nebular minor axis. A displacement of  $\simeq 0''.05$  (120 AU) is obtained from the [NII] and H $\alpha$  images with respect to the center of the toroid, and from the H $\alpha$  and [OIII] images with respect to the center of the inner shell.

The high resolution of the HST images allows us to study the structure of C1–C4 and D in detail. C1 and C3 consist each of two small and close knots. In the case of C1, the long-slit spectra (M95, see his Fig.4) show two knots at different radial velocity and separated by  $\simeq 0''.9$ , in agreement with the HST [NII] image. In C2 no evidences for more than a knot are found, taking into account that part of the emission near the position of C2 corresponds to structure D (see M95). In the case of C4 a bright knot can be distinguished near the SE lobe and a fainter one at  $\simeq 4''$  from the center, which could be related to structure D. D appears as several bow-shock-like structures at different orientations.

Figure 4 presents image ratios deduced from the ground-based images, which have been used to

study the global variations of the excitation conditions in Hu 2-1. A wealth of structure is observed in these images. The innermost nebular regions are of relatively high excitation whereas the edges of the bipolar lobes and the toroid present a relatively low excitation. Point-symmetry in the lobes can also be recognized in the excitation conditions. Low excitation is observed in C1 to C4 and D. The variation of the excitation along the nebular minor axis is particularly interesting. Close to the edges of the toroid (along PA  $50^\circ$ ), we observe a relatively low excitation zone. The excitation increases outwards and two high-excitation maxima are observed at  $\simeq 2''.5$  from the center. These maxima are very prominent in [OIII]/[NII] and seem to form part of a distinct high-excitation circular region which is better observed in [OIII]/H $\alpha$ . Beyond this high-excitation region, H $\alpha$  dominates in a band along the equatorial plane up to  $\simeq 6''$  from the center. The ratio maps also show a region dominated by H $\alpha$  at PA  $\simeq 80^\circ$  up to  $\simeq 4''$  from the center (see above).

## 2.2. Radio observations

The observations were carried out with the Very Large Array (VLA) of the National Radio Astronomy Observatory (NRAO)<sup>2</sup> during 1995 July with the VLA in its A configuration. The data were obtained in the spectral line mode in order to study the H92 $\alpha$  recombination line ( $\nu = 8309.383$  MHz [3.6 cm]). We used a bandwidth of 6.25 MHz with two circular polarizations centered at the LSR velocity of  $33.3 \text{ km s}^{-1}$  and 63 channels of 97.7 kHz ( $\simeq 3.5 \text{ km s}^{-1}$ ) wide each plus a continuum channel (channel 0) which contains the central 75% of the total bandwidth. Integration time was  $\simeq 2.5$  hours with  $\simeq 20\%$  of this time spent in calibration. 3C 286 and 1923+210 were used as flux and phase calibrators, respectively. Calibration and image processing were carried out with the Astronomical Image Processing System (AIPS) of the NRAO. Continuum emission at 3.6 cm and H92 $\alpha$  emission were detected from Hu 2-1. We show in Figure 5 a grey-scale map of the 3.6 cm continuum emission obtained with uniform weighting of the (u,v) data (beam =  $0''.20 \times 0''.19$ , PA =  $-14^\circ$ ). In Figure 6, we show contours of the H92 $\alpha$  emission obtained by adding all channels in which line emission is detected (from 19 to  $51 \text{ km s}^{-1}$ ), superposed on a 3.6 cm continuum map made with natural weighting and a Gaussian taper of  $500 \text{ k}\lambda$  (beam =  $0''.42 \times 0''.40$ , PA =  $60^\circ$ ). The continuum flux density at 3.6 cm is  $\simeq 110 \text{ mJy}$ , compatible with the value obtained by KA93. The H92 $\alpha$  flux density is  $\simeq 3.9 \text{ mJy}$ .

The 3.6 cm continuum map (Fig.5) shows the innermost regions of Hu 2-1 in considerable detail. The bright regions separated  $\simeq 1''$  at PA  $\simeq 50^\circ$  correspond to the outer edges of the toroid. The inner shell, identified by KA93, can be distinguished with a size of  $\simeq 0''.35$  and with the major axis near PA  $320^\circ$ . In our map, it shows open ends and a clear point-symmetric brightness distribution. Detection of H92 $\alpha$  emission is restricted to a region of  $\simeq 0''.5$  in radius apparently coinciding with the inner shell (Fig.6). We note that given the intensity of the continuum emission in the outer edges

---

<sup>2</sup>The NRAO is a facility of the National Science Foundation operated under a cooperative agreement with Associated Universities, Inc.

of the toroid, one would expect to detect H92 $\alpha$  emission from these positions as well. However, the continuum emission towards the edges of the toroid is probably optically thick, preventing the detection of H92 $\alpha$  emission.

Figure 7 presents the H92 $\alpha$  line profile. The LSR central velocity and the line width (FWHM) of the H92 $\alpha$  emission have been determined by means of a single-gaussian fit and are listed in Table 1. Given the reduced S/N of the profile, the deduced systemic velocity ( $V_{LSR} \simeq 37 \pm 2 \text{ km s}^{-1}$ ) is compatible with that deduced from optical emission lines (see below). Because of the low S/N in the individual channels, a detailed study of the kinematics in H92 $\alpha$  is not possible. In order to increase the S/N, we have added the blueshifted channels and the redshifted channels with respect to the systemic velocity as deduced from the optical lines. The result is presented in Figure 8. Blueshifted emission appears slightly displaced towards the N-NW, with respect to the emission center in the continuum image, whereas redshifted emission is displaced towards the S-SE.

Estimates for the electron density and electron temperature were obtained from the continuum and line emission following the formulation by Mezger & Henderson (1967), assuming the gas is in LTE and from the observed line-to-continuum ratio  $T_C/T_L$  of  $\sim 12.5$ . The results are listed in Table 1. The values obtained for the electron density and temperature are similar to those obtained from optical emission lines (see M95 and references therein).

### 2.3. Long-slit spectroscopy

Long-slit spectra were obtained in 1998 August with IACUB<sup>3</sup> at the NOT. A filter was used to isolate the H $\alpha$  and [N II]6583 emission lines. Two spectra were obtained at PAs 320 $^\circ$  and 351 $^\circ$  with the slit centered on the object. Exposure time was 900 s for each spectrum. A Th-Ar lamp was used for wavelength calibration. The spectral resolution (FWHM) is  $\simeq 8 \text{ km s}^{-1}$ . Seeing was  $\simeq 1.4''$ . The data were reduced using standard procedures within the IRAF<sup>4</sup> and MIDAS packages. The error in absolute radial velocity is estimated to be  $\simeq \pm 1.2 \text{ km s}^{-1}$ . However, the internal accuracy in each long-slit spectrum is much better,  $\simeq \pm 0.15 \text{ km s}^{-1}$ . Contour plots of the [NII]6583 emission line, in a position–velocity representation, are shown in Figure 9. As compared with the spectra presented by M95, the new ones, although with poorer spatial resolution, have a higher spectral resolution and provide information about the bipolar knots C3–C4.

Table 2 lists different parameters of the knots C1 to C4 (PA, radial velocity, angular position and spectral and angular widths) obtained from the spectra. Radial velocities and angular positions refer to the centroid of the knots. The radial velocities are quoted with respect to the systemic

---

<sup>3</sup>The IACUB uncrossed echelle spectrograph was built in a collaboration between the IAC and the Queen’s University of Belfast

<sup>4</sup>IRAF is distributed by the National Optical Astronomy Observatory, operated by the Association of Universities for Research in Astronomy, Inc. (AURA) under cooperative agreement with the National Science Foundation

velocity of the main nebular shell [ $V_{sys}(\text{shell})$ ] (hereafter considered as the toroid and bipolar lobes) for which we deduce  $V_{LSR} = 34.5 \pm 1.2 \text{ km s}^{-1}$  ( $V_{\odot} = 15.1 \text{ km s}^{-1}$ ) in agreement with previous determinations (Schneider et al. 1983; M95; Durand et al. 1998). Spatial positions have been determined with respect to the central star, represented by the position of the maximum of the stellar continuum in the two-dimensional frames, with a precision of  $\simeq \pm 0''.1$ . The results for C1–C2 are compatible with those obtained by M95, the small differences being due to the fact that in Table 2 the parameters refer to the centroid of the knots, whereas M95 considered the peak intensity. In addition, the new spectra show that C3–C4 constitutes a system of highly collimated bipolar knots.

The following results are noticed from Table 2. The radial velocity of the NW knots C1 and C3 is systematically higher than that of their corresponding SE counterparts C2 and C4. In particular, the radial velocity of C1 is  $11 \text{ km s}^{-1}$  higher than that of C2 and the radial velocity of C3 is  $16 \text{ km s}^{-1}$  higher than that of C4. The radial velocity decreases with the distance in C1 and C3. In fact, the position–velocity maps (Fig.8) suggest that two knots at different velocities are present in C3. Within C2 and C4 the radial velocity is constant (see also M95). C1–C2 are located at larger distance from the central star than C3–C4. However, differences in the distance for the knots in a particular pair do not seem to be significant. C1 and C3 present a higher velocity width than C2 and C4. This can be explained taking into account that C1 and C3 consist of two small knots at different velocity (see above) and, therefore, the velocity width results from the superposition of two knots which are not spatially resolved in our spectra.

The results for the toroid and bipolar lobes are compatible with those obtained by M95. In the case of D we confirm the previous results, in particular, its very low radial velocity (between  $-2$  and  $+2 \text{ km s}^{-1}$ , see M95 for details).

### 3. Discussion

In the following we will discuss possible interpretations for the data presented above, testing the scenario of a binary system at the center of Hu 2-1.

#### 3.1. Shaping of the inner and bipolar shells

The data suggest that the inner shell could be (1) an elliptical, independent shell (see KA93), (2) the inner “walls” of the toroid or (3) a second, inner toroid concentric with the outer one. The kinematics of this shell can be used to decide between these possible interpretations. As already mentioned, the H92 $\alpha$  emission seems to be related to the inner shell. If this shell represents the inner walls of the toroid or a second toroid concentric with the outer one, it would be expected to detect the H92 $\alpha$  emission blueshifted (redshifted) towards the SE (NW) part of the toroid, according to its inclination (M95). However, the opposite is found (§2.2, Fig.8) as expected if the H92 $\alpha$

emission would trace an expanding ellipsoidal shell with the NW (SE) part blueshifted (redshifted) as the bipolar lobes or a toroid with a different inclination as the outer one. Nevertheless, these interpretations do not explain the point-symmetry of the inner shell, which suggests the existence of a non-spherical wind interior to the inner shell, at scales  $\leq 0''.35$ , which is not oriented along the major nebular axis and impacts the inner shell at certain angle. It is possible that the H92 $\alpha$  emission could be tracing a bipolar outflow interior to the inner shell. The foreseen upgrading of the VLA will certainly allow us to study with great sensitivity and high resolution the innermost regions of the nebula.

With regards to the bipolar shell, the equatorial toroid expands at  $\simeq 15 \text{ km s}^{-1}$  in [NII] (M95) and the HST [NII] image indicates a size of  $\simeq 1''.1$ , so that its kinematic age is  $\simeq 410 \text{ yr}$ . The bipolar lobes expand at  $\simeq 30 \text{ km s}^{-1}$  (M95) and the HST images indicate a maximum radius of  $\simeq 2''.2$  at PA  $330^\circ$ . The bipolar axis is tilted  $\simeq 37^\circ$  with respect to the plane of the sky. With these numbers, the kinematic age of the bipolar lobes results to be  $\simeq 1000 \text{ yr}$ , much larger than the age of the toroid. This difference can be explained if the kinematics of the lobes is more complex than previously assumed (M95). In fact, the maximum size of the lobes is observed along PA  $330^\circ$  where the largest departures from axial symmetry are observed. It is plausible that these regions are expanding at a higher velocity than  $\simeq 30 \text{ km s}^{-1}$  and/or are tilted at an angle different from  $37^\circ$ . Therefore, the kinematic age of the toroid probably is more representative for the age of the bipolar shell.

In any case, the shape of the bipolar lobes points out to a bipolar wind interior to the main shell. In an idealized model of interacting stellar winds (see Zhang & Kwok 1998 and references therein), the lobes in a bipolar PN should be symmetric with respect to the bipolar axis. This is not the case for the lobes in Hu 2-1, which show clear departures from axis-symmetry. As in the case of the inner shell, we propose the existence of an interior bipolar wind which is not oriented along the main nebular axis, but impacts the lobes at certain angle, so that the lobes are inflated in an asymmetric (with respect to the main nebular axis) but point-symmetric (with respect to the central star) manner. Interaction of collimated outflows with shells has been suggested to occur in other PNe (Sahai & Trauger 1998; Miranda et al. 1999; Vázquez et al. 1999, 2000). We note that in the case of Hu 2-1, however, knots C1 to C4 do not seem to be involved in shaping the bipolar lobes, because evidence for interaction between the knots and lobes cannot be recognized in our data. If interaction would have existed, one would expect strong deformations of the lobes at the PAs where the knots are detected (see, e.g., Miranda et al. 1999), which is not observed. The origin of the interior bipolar wind is difficult to elucidate from the observed geometry alone. It could be either that the fast stellar wind from the central star is anisotropic in origin or that two winds are present: an isotropic fast stellar wind from the central star and an intrinsically bipolar wind from a companion.



### 3.2. The structure of the equatorial plane

The image ratio maps show an equatorial zone within the halo, which is characterized by peculiar line ratios, particularly those involving  $H\alpha$ . This suggests the existence of a flat equatorial region with physical conditions different from those in other parts of halo. A plausible interpretation for this equatorial region is that it is related to, and traces anisotropic mass ejection during the AGB phase of the Hu 2-1 progenitor. In fact, for an expansion velocity of  $10 \text{ km s}^{-1}$ , the kinematic age of the flat region is  $\simeq 7000 \text{ yr}$ , much larger than that of the main shell. Taking into account that the transition time from AGB to PN is  $\simeq 2000\text{--}3000 \text{ yr}$  and the evolutionary time in the AGB is  $\simeq 10^6 \text{ yr}$ , the formation of this region has occurred in the very late stages of AGB evolution. The distinct high-excitation region within the halo is younger,  $\simeq 2800 \text{ yr}$ , also assuming a velocity of  $10 \text{ km s}^{-1}$ . This region could represent the final ejection in the AGB before the object entered in its proto-PN phase. The high-excitation in this region could be related to hardening of the radiation as observed in high-excitation haloes of PNe (Guerrero & Manchado 1999).

Different mechanisms have been suggested to produce anisotropic mass loss during the AGB, including stellar rotation, magnetic fields, non-radial pulsations and binariety (Soker 1996 and references therein; García-Segura et al. 1999; Mastrodemos & Morris 1999). In many cases, the presence of a companion is required either to spin up the envelope of the AGB star or to deflect the mass towards the equatorial plane (see, e.g., Soker 1996). However, García-Segura et al. (1999) have recently modelled single stars rotating at near-critical rotation rates at the end of AGB. These models also produce ejection towards the equatorial plane and, when combined with an interacting winds scenario and magnetic fields, they are capable to account for the large variety of shapes observed in PNe (García-Segura et al. 1999). In the case of Hu 2-1, the simple detection of an equatorial ring-like structure ejected during the end of AGB does not allow us to discriminate between single star or binary scenarios.

### 3.3. The off-center position of the central star

Off-center central stars are observed in many PNe (see Soker 1999 and references therein). We compare Hu 2-1 with MyCn 18 (Sahai et al. 1998), which are considered to be at a similar distance. In both cases, the central star is displaced along the nebular minor axis. In Hu 2-1, the displacement is  $\simeq 120 \text{ AU}$  while larger displacements, between 270 and 1150 AU, are found in MyCn 18 with respect to different nebular structures (Sahai et al. 1998). A possibility to explain a displaced central star is relative proper motion of the central star and nebula. In Hu 2-1 this possibility can be ruled out because the proper motion vector of the nebula is perpendicular to the direction of displacement (Acker et al. 1998). Another possibility to be considered is binariety of the central star. Soker (1994) and Soker et al. (1998) model the influence in the nebular morphology of wide and eccentric close binaries, respectively. In both cases, off-center central stars are predicted. Hu 2-1 fits much better the eccentric scenario because (1) the displacement is observed along the minor

nebular axis and (2) bipolar PNe could be related to eccentric binaries (see Soker et al. 1998). According to these authors, orbital separations of 7–80 AU and orbital periods of 15–500 yr are suggested for this kind of eccentric close binaries (see § 3.5).

### 3.4. Collimated outflows and possible detection of orbital motion

The new data have revealed the existence of multiple collimated knots in Hu 2-1 at different directions. Whereas C1–C2 and C3–C4 represent the typical bipolar collimated outflows observed in PNe, the nature of D is less clear. The bow-shock appearance suggests that D could represent a series of collimated outflows. In this case, the outflows should have been monopolar and either they move almost perpendicular to the line of sight or its expansion velocity is very low. In any case, D does not share the general inclination of the nebula. We note that D is located towards the SE, coinciding with the direction of the proper motion of Hu 2-1 (Acker et al. 1998). Therefore, it is possible that the formation of D could be related to interaction of the nebula with the interstellar medium.

The properties of the collimated outflows C1–C2 and C3–C4 suggest a precessing ejection source. These kind of outflows is much better accommodated by a binary scenario than into a single-star one (see below). Single-star models have been able to explain jets in PNe if stellar rotation and magnetic fields are considered (García-Segura et al. 1999). This model produces jets along the main nebular axis. If precessing jets are to be explained within these models, a companion to the central star is required (García-Segura 1997). Therefore, the mere presence of collimated outflows at different directions in Hu 2-1 suggests a binary central star.

The most striking result concerning the bipolar outflows is the systematic difference between the radial velocities of the two knots in each bipolar pair. This could be attributed to differences in the ejection velocity (M95). In this case, systematic differences in position of the knots with respect to the central star would be expected, but they are not observed. Another possibility is deceleration of the knots by interaction with nebular material. If so, deceleration should have been more conspicuous in C2 and C4, the knots with lower radial velocity. However, evidence for deceleration exists in C1 and C3 which show an internal decrease of the radial velocity (see §2.3), but not in C2 and C4 in which the radial velocity is constant. We also note that a combination of different ejection velocity, different ejection angle and selective deceleration is highly improbable because of the very peculiar combination of these parameters necessary to explain the systematic differences in radial velocity and the symmetric location of the knots in each pair with respect to the central star.

In order to explain these results, we consider a completely different and novel point of view, namely, that the differences in radial velocity arise only because we have measured them with respect to  $V_{\text{sys}}(\text{shell})$  which, in this case, is a misleading reference system for the collimated outflows. In other words, we suggest that the systemic velocity of the main nebular shell does not coincide with

the systemic velocity of the collimated knots. Remarkably, this situation is what one would expect from a binary ejection source. The systemic velocity of the main nebula is related to material ejected during the last stages of the AGB phase averaged over a relatively large time span and over many orbits. In a first approximation, the average velocity of the ejection will be the same in all directions and the systemic velocity will not contain information about the orbital velocity or about a particular orbital position (but see below). The collimated knots, however, can be considered as “instantaneous” ejections, given its compactness. Their space velocities will contain two components: the component due to the own ejection velocity and the component due to the “instantaneous” orbital velocity at the time of ejection. The component due to the orbital velocity will be added with the same sign to the component due to its own ejection velocity in each knot of a bipolar pair. As a consequence of the additional orbital component of the velocity, the systemic velocity of the knots will be shifted with respect to  $V_{\text{sys}}(\text{shell})$ .

The data in Table 2 allow us to obtain the systemic velocity and the radial velocities of the knots with respect to their own systemic velocity. For C1–C2 we obtain  $V_{\text{sys}}(\text{C1–C2}) = 29 \text{ km s}^{-1}$  and a radial velocity of  $\pm 53.5 \text{ km s}^{-1}$  with respect to  $V_{\text{sys}}(\text{C1–C2})$ . For C3–C4,  $V_{\text{sys}}(\text{C3–C4})$  is  $26.5 \text{ km s}^{-1}$  and the radial velocity is  $\pm 58 \text{ km s}^{-1}$  with respect to  $V_{\text{sys}}(\text{C3–C4})$ . The three systemic velocities  $V_{\text{sys}}(\text{C1–C2})$ ,  $V_{\text{sys}}(\text{C3–C4})$  and  $V_{\text{sys}}(\text{shell})$  are represented in Fig.9. Both  $V_{\text{sys}}(\text{C1–C2})$  and  $V_{\text{sys}}(\text{C3–C4})$  are blueshifted with respect to  $V_{\text{sys}}(\text{shell})$  by  $5.5$  and  $8 \text{ km s}^{-1}$ , respectively. These values are noticeable larger than the relative errors (§2). In addition,  $V_{\text{sys}}(\text{C1–C2})$  and  $V_{\text{sys}}(\text{C3–C4})$  are almost identical to each other within the absolute errors. In the following, we will consider as radial velocity of the knots that referred to their own systemic velocity.

Estimates for the expansion velocity, distance to the central star and kinematic age of the collimated outflows can be obtained if the inclination angle is known. The location of C1–C2 along the major nebular axis suggests that C1–C2 move along that axis (M95). However, this must not be necessarily true. For instance, some parts of D also project along the major axis but they move in a completely different direction. In addition, we note that for inclinations of C1–C2  $\leq 40^\circ$ , the kinematic age of the knots is lower than that of the toroid. This would imply interaction of the collimated knots with the shell, which is not observed (see above). Therefore, we will assume a range of  $40^\circ$ – $60^\circ$  for the inclination of C1–C2 and a constant velocity for the two pairs. We obtain a range of outflow velocities between  $60$ – $85 \text{ km s}^{-1}$  and a range of kinematic ages for C1–C2 between  $520$ – $1100 \text{ yr}$ . The difference of kinematic ages between C1–C2 and C3–C4 is  $\simeq 15$ – $100 \text{ yr}$ .

### 3.5. Binary parameters and implications for jet formation in Hu 2-1

The available information can be used to constrain the characteristics of the binary central star in Hu 2-1. From the simple model outlined above (§3.4), it can be easily demonstrated that

$$V_{\text{sys}}(\text{knots}) - V_{\text{sys}}(\text{shell}) = V_{\text{orb}} \times \cos(\gamma) \times \cos(i) \quad (1)$$

where  $V_{\text{orb}}$  is the orbital velocity at the time of ejection,  $\gamma$  is the angle between the orbital velocity vector and the line of sight and  $i$  is the inclination angle of the orbital plane with respect to the line of sight. For  $V_{\text{sys}}(\text{knots}) - V_{\text{sys}}(\text{shell})$  we obtain  $5.5\text{--}8 \text{ km s}^{-1}$ . In addition, it is reasonable to assume that the orbital plane coincides with the equatorial plane of the nebula, which is tilted  $\simeq 37^\circ$ . With these assumptions, we obtain  $V_{\text{orb}} \times \cos(\gamma) \simeq 10 \text{ km s}^{-1}$ , which is a lower limit to the orbital velocity. For masses  $M_1 + M_2$  in the range  $1\text{--}3 M_\odot$ , we obtain upper limits for the orbital separation of  $\simeq 9\text{--}27 \text{ AU}$  (assuming circular orbit, see also below) and for the period of  $\simeq 25\text{--}80 \text{ yr}$ . It is worth noting that these orbital parameters are in the range of those expected from the displacement of the central star (§2.1). Therefore, the true orbital separation and period should not be much lower than the obtained upper limits, which also implies that the orbital velocity should not be much larger than the deduced value.

Two basic binary scenarios have been suggested to explain the generation of precessing collimated outflows in PNe. A scenario is that of a mass transferring binary (Morris 1981; Soker & Livio 1994; Mastrodemos & Morris 1998). In this scenario, mass lost from the AGB star is partially captured by the secondary forming an accretion disk around it, from which collimated outflows are produced. Precession of the accretion disk will result in changes of the direction of the collimated outflows. A different scenario is considered by Soker & Livio (1994) and Soker (1996), in which a disk is formed around the AGB nucleus by Roche lobe overflow and destruction of a stellar or substellar companion. In this case, the jets emanate from the AGB star. Radiation may induce self-warping of the disk so that the disk precesses originating precessing outflows (Livio & Pringle 1996). In the first case, models by Mastrodemos & Morris (1998, 1999) indicate that accretion onto the secondary is effective at large orbital separations ( $\simeq 24 \text{ AU}$ ). The second scenario requires orbital separations  $\leq 2 R_\odot$  for the secondary being destroyed (Soker 1996; Reyes-Ruiz & López 1999). The binary parameters deduced for Hu 2-1 clearly favor a mass transferring binary scenario with the collimated ejection generating from an accretion disk around the secondary. Furthermore, the ejection of material towards the equatorial plane is also compatible with a binary of these characteristics (Mastrodemos & Morris 1999).

In the previous calculations, we have assumed circular orbit. This is not necessarily true. In fact, the off-center position of the central star points out to an eccentric binary (§3.3). In this case, the ejection velocity of the AGB wind may depend on the orbital position (Soker 1998; Mastrodemos & Morris 1998) so that the measured systemic velocity of the nebula will contain some information about the orbital velocity. However, the displacement of the central star in Hu 2-1 is small as compared, for instance, with that in MyCn 18. In fact, the displacement amounts  $\simeq 5\text{--}15\%$  in terms of the size of the outer edges of the toroid and inner shell, respectively, which is smaller than the displacement observed in MyCn 18 ( $\simeq 25\%$ ). This suggests that the ellipticity is small and/or that there is a small dependence of mass loss with the orbital position. However, without regards of these considerations, the systemic velocities of the two pairs are very similar to each other. From this result and taking into account that the amplitude of the radial velocity curve could be  $\sim 20 \text{ km s}^{-1}$  (see above), it can be concluded that collimated ejection occurs at a particular

orbital phase and may be a “periodic” phenomenon. This suggests that mass accretion is enhanced at some points of the orbit, e.g., through passage by the periastron so that “massive” collimated outflows in the form of bright knots are generated. This conclusion is supported by the similarity between the difference of kinematic ages of the two collimated pairs (15–100 yr) and the orbital period (25–80 yr). At different orbital positions, after “massive” collimated ejection occurs, the bipolar outflow could still be active but with different properties (e.g., mass loss, velocity, direction, collimation angle) so that collimated knots are not generated. However, the bipolar outflow may still be capable to shape the bipolar lobes and the inner shell.

The orbital parameters deduced in Hu 2-1 are remarkably similar to those of symbiotic stars (e.g. Seaquist & Taylor 1990). Some symbiotic stars exhibit bipolar shells, equatorial disks and collimated outflows. In particular, we find remarkable similarities between Hu 2-1, R Aqr and HM Sge. The orbital separation and period in these symbiotic are: 18 AU and 44 yr in R Aqr and 25 AU and 90 yr in HM Sge (Hollis et al. 1997; Richards et al. 1999). Although these parameters are rough estimates, they compare very well to those of Hu 2-1. Moreover, “precessing” collimated outflows are present in R Aqr and HM Sge as well as a bipolar shell and an equatorial ring-like structure (see Solf 1984; Solf & Ulrich 1985; Hollis et al. 1990; Corradi et al. 1999). We also note that Solf & Ulrich (1985) found in R Aqr a difference of  $13 \text{ km s}^{-1}$  between the systemic velocity of the two bipolar shells, which was attributed to orbital motion. This suggestion is supported by the velocity semi-amplitude for the Mira in R Aqr (Hollis et al. 1997). The possible evolutionary relationship of symbiotic stars with PNe has already been pointed out (Corradi et al. 1999 and references therein). From the results presented in this paper, we suggest that Hu 2-1 represents the result of the evolution of a symbiotic star similar to R Aqr and HM Sge, after the AGB star has evolved towards a central star of PNe.

#### 4. Conclusions

We have carried out a multiwavelength observational study of the PN Hu 2-1 based on a set of optical/radio data obtained at high spectral and/or spatial resolution. These data have allowed us to identify many structural components in this complex PN. The main shell of Hu 2-1 is bipolar and consists of a toroid and two point-symmetric lobes which also exhibit noticeable departures from axial symmetry. Inside the toroid, an inner point-symmetric shell is observed. Two bipolar pairs of low-excitation knots are identified at different directions and correspond to collimated outflows. Several monopolar, low-excitation bow-shocks-like structures are observed on one side of the nebula. We confirm the existence of an extended halo around the main nebula. This halo contains a distinct, extended equatorial disk-like region with peculiar excitation conditions.

The early formation of Hu 2-1 seems to be dominated by mass ejection towards the equatorial plane. This anisotropic mass loss process, resulting in the formation of a flat region within the halo, appears to have been active from the very late stages of AGB evolution up to the onset of the proto-PN phase. However, during the proto-PN and/or PN phase, variable, “precessing”

bipolar collimated outflows appear as the dominant formation mechanism of the nebula. This kind of outflows can be identified not only as two systems of highly collimated bipolar knots at different orientations but they could also be recognized in the point-symmetry of the bipolar lobes and inner shell and in the departure from axis-symmetry of the bipolar lobes. We also note that interaction with the interstellar medium could also be involved in the formation of the monopolar structures.

The whole set and the consistence of the different results provide strong support to conclude that a binary central star has been involved in the formation of Hu 2-1. First-order estimates for the orbital parameters (separation  $\sim 9\text{--}27$  AU, period  $\sim 25\text{--}80$  yr) have been deduced from the observed kinematics and a simple binary model. These parameters suggest that the central star of Hu 2-1 is a mass transferring binary in which collimated ejections are generated from an accretion disk around a companion. There are many similarities between Hu 2-1 and symbiotic stars as, e.g., R Aqr and HM Sge, which lead us to suggest that Hu 2-1 may be the descendent of this kind of binary stars.

We suggest that a precise comparison of the systemic velocity of collimated outflows and main shell in other PNe may be a powerful method to detect the effects of orbital motion in a binary central star and/or to place strong constraints on the possible nature of the central star and on the scenario for the generation of collimated outflows.

## Acknowledgments

We thank our referee for his/her comments which have been very useful to improve the presentation and interpretation of the data. We are very grateful to E. Alfaro, G. Anglada, A. Claret and E. Pérez for useful comments and discussions. LFM and JMT are supported partially by DGEIC PB98-0670-C02 and Junta de Andalucía (Spain). MAG is supported partially by DGEIC of the Spanish Ministerio de Educación y Cultura. YG acknowledges financial support from DGAPA-UNAM and CONACyT-Mexico. RV acknowledges financial support from CONACyT grant I32815E (Mexico). This work has been supported partially by the Programa de Cooperación Científica con Iberoamérica.

## REFERENCES

- Aaquist O.B., Kwok S., 1990, *A&AS*, 84, 229
- Acker A., Fresneau A., Pottasch S.R., Jasniewicz G., 1998, *A&A*, 337, 253
- Arkhipova, V.P., Kostyakova E.B., Noskova R.I., 1994, *PAZh*, 20, 122
- Bond H.E., 2000, in *ASP Conf. Ser.*, vol. 199, J.H. Kastner, N. Soker & S. Rappaport (eds.), 115
- Ciardullo R., Bond H.E., Sipior M.S., Fullton L.K., Zhang C.-Y., Schaefer K.G., 1999, *AJ*, 118, 488
- Corradi R.L.M., Ferrer O.E., Schwarz H.E., Brandi E., García L., 1999, *A&A*, 348, 978
- Durand S., Acker A., Zijlstra A., 1998, *A&AS*, 132, 13
- García-Segura G., 1997, *ApJ*, 489, L189
- García-Segura G., Langer N., Rózycka M., Franco J., 1999, *ApJ*, 517, 767
- Guerrero M.A., Manchado A., 1999, *ApJ*, 522, 378
- Hollis J.M., Pedelty J.A., Lyon R.G., 1997, *ApJ*, 482, L85
- Hollis J.M., Wagner R.M., Oliverson R.J., 1990, *ApJ*, 351, L17
- Kwok S., Aaquist O.B., 1993, *PASP*, 105, 1456 (KA93)
- Kostyakova E., 1992, *PAZh*, 18, 802
- Livio M., Pringle J.E., 1996, *ApJ*, 465, L55
- Mastrodemos N., Morris M., 1998, *ApJ*, 497, 303
- Mastrodemos N., Morris M., 1999, *ApJ*, 523, 357
- Mezger P.G., Henderson A.P., 1967, *ApJ*, 147, 490
- Morris M., 1987, *PASP*, 99, 115
- Miranda L.F., 1995, *A&A*, 304, 531 (M95)
- Miranda L.F., 1999, in *ASP Conf. Ser.*, vol.188, p. 257
- Miranda L.F., Vázquez R., Corradi R.L.M., Guerrero M.A., López J.A., Torrelles J.M., 1999, *ApJ*, 520, 714
- Reyes-Ruiz M., López J.A., 1999, *ApJ*, 524, 952
- Richards A.M.S., Bode M.F., Eyres S.P.S., Kenny H.T., Davis R.J., Watson S.K., 1999, *MNRAS*, 305, 380

- Sahai R., Dayal A., Watson A.M., et al., 1999, AJ, 118, 468
- Sahai R., Trauger J.T., 1998, AJ, 116, 1357
- Schneider S.E., Terzian Y., Purgathofer A., Perinotto M., 1983, ApJS, 52, 399
- Seaquist E.R., Taylor A.R., 1990, ApJ, 349, 313
- Soker N., 1994, MNRAS, 270, 774
- Soker N., 1996, ApJ, 468, 774
- Soker N., 1998, ApJ, 496, 833
- Soker N., 1999, AJ, 118, 2424
- Soker N., Livio M., 1994, ApJ, 421, 219
- Soker N., Rappaport S., Harpaz A., 1998, ApJ, 496, 842
- Solf J., 1984, A&A, 139, 296
- Solf J., Ulrich , 1985, A&A, 148, 274
- Zhang C.Y., Kwok S., 1998, ApJS, 117, 341
- Vázquez R., López J.A., Miranda L.F., Torrelles J.M., Meaburn J., 1999, MNRAS, 308, 939
- Vázquez R., López-Martín L., Miranda L.F., Esteban C., Torrelles J.M., Arias L., Raga A.C., 2000, A&A, 357, 1031



**Figure captions**

**Figure 1.**  $H\alpha$ , [OIII]5007 and [NII]6583 contour maps of Hu 2-1 from the ground-based images. North is up, east to the left. The contours are logarithmic separated by a factor 1.78 in intensity and have been chosen in order to show up the main features of the nebula. The identified morphological components are indicated in the [NII] image (see text).

**Figure 2.** HST image of Hu 2-1 obtained in the [NII]6583 line. Two different grey levels have been chosen in order to show both the faint and bright nebular structures. The morphological components are indicated (see also Fig.1).

**Figure 3.** Grey-scale map of the central regions of Hu 2-1 as observed in the  $H\alpha$  line with the HST. The inner shell is indicated.

**Figure 4.** Grey-scale ratio maps of Hu 2-1 obtained from the images in Fig.1. North is up, east to the left. In each image ratio, black regions refer to high ratios, white regions refer to low ratios.

**Figure 5.** Grey-scale representation of the 3.6 cm continuum map with uniform weighting (beam  $0''.20 \times 0''.19$ , PA  $-14^\circ$ ). The grey levels (top scale) are in  $\text{mJy beam}^{-1}$ .

**Figure 6.** Contour map of the velocity-integrated  $H92\alpha$  emission (solid line) superposed on a contour map of the 3.6 cm radio continuum emission (dashed line) made with natural weighting and a Gaussian taper of  $500 \text{ k}\lambda$  which resulted in a synthesized beam of  $0.42 \times 0.40$ , PA  $60^\circ$ . The levels for  $H92\alpha$  are 30, 40, 50, 60, 70, 80, 90 and 95 percent of the maximum of  $50.2 \text{ mJy beam}^{-1} \text{ km s}^{-1}$ . Radio continuum contour levels are 3, 5, 7, 9, 15, 30, 50, 70, 90, 100, 150 and  $200 \times 7.1 \times 10^{-2} \text{ mJy beam}^{-1}$ , the rms noise of the map. The peak position of the radio continuum map is  $\alpha(1950) = 18^h 47^m 38^s.60$  and  $\delta(1950) = 20^\circ 47' 08''.0$ .

**Figure 7.**  $H92\alpha$  emission profile. The dotted line shows a Gaussian fit to the line profile.

**Figure 8.** Contour maps of the  $H92\alpha$  emission for the two velocity intervals indicated in the upper right corner. Solid contours represent blueshifted emission, dashed contours represent redshifted emission with respect to the systemic velocity.

**Figure 9.** Position-velocity contour maps of the [NII]6583 long-slit spectra. Position angle of the slit is indicated in the upper right corner. The contour are logarithmic separated a factor 2 in intensity. The knots C1, C2, C3 and C4 are indicated. The position of the central star is represented by the position of the intensity maximum of the continuum.  $V_{\text{sys}}(\text{shell})$  indicates the systemic velocity of the main nebular shell whereas  $V_{\text{sys}}(\text{C1-C2})$  and  $V_{\text{sys}}(\text{C3-C4})$  indicate the systemic velocity of the two pairs of compact knots (see text for details).

**Table 1: Physical parameters of Hu 2-1<sup>a</sup>**

Parameter	Value
$S_\nu(\text{continuum})$ (mJy) <sup>b</sup>	$110 \pm 1$
$S_\nu(\text{line})$ (mJy) <sup>b</sup>	$3.9 \pm 0.3$
$V_{LSR}$ (km s <sup>-1</sup> ) <sup>c</sup>	$37 \pm 2$
$\Delta V_L$ (km s <sup>-1</sup> ) <sup>c</sup>	$33 \pm 2$
$T_e$ (K) <sup>d</sup>	$7000 \pm 500$
$N_e$ (cm <sup>-3</sup> ) <sup>e</sup>	$5900 \pm 100$

<sup>a</sup> Obtained from continuum and H92 $\alpha$  observations at 3.6 cm following the formulation by Mezger & Henderson (1967).

<sup>b</sup> Total continuum and integrated line flux density.

<sup>c</sup> Systemic velocity and velocity width of the H92 $\alpha$  line, determined by a Gaussian fit.

<sup>c</sup> Electron temperature, assuming a distance of 2.35 kpc (see text).

<sup>e</sup> Electron density.

**Table 2: Parameters of the knots C1, C2, C3 and C4<sup>a</sup>**

Knot	PA	$V_r$ <sup>b</sup>	$X$ <sup>c</sup>	$\Delta V$ <sup>d</sup>	$\Delta X$ <sup>e</sup>
	(degrees)	(km s <sup>-1</sup> )	(arcsec)	(km s <sup>-1</sup> )	(arcsec)
C1	320	-59	3.0	28	1.4
C2	140	+48	3.0	17	1.5
C3	351	-66	2.5	29	1.3
C4	171	+50	2.4	19	1.6

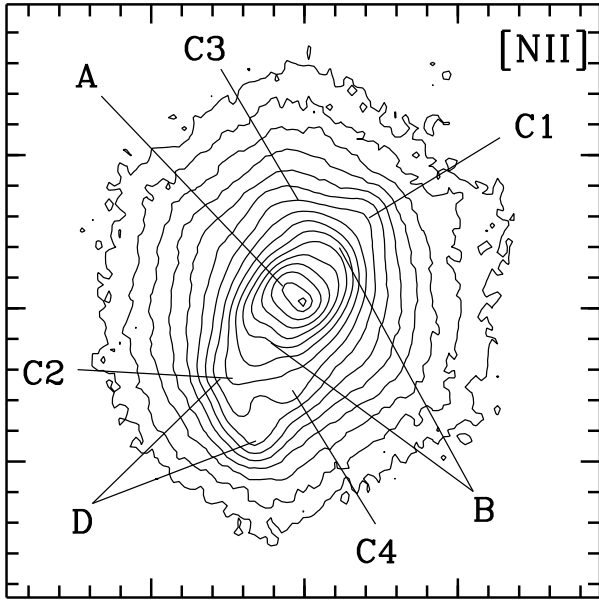
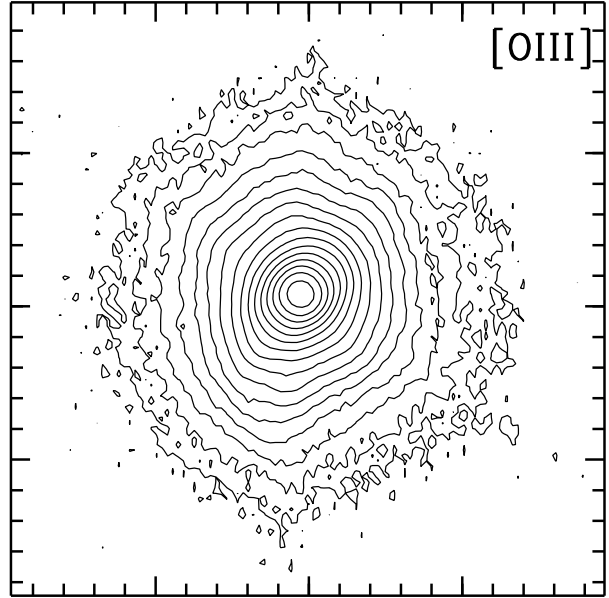
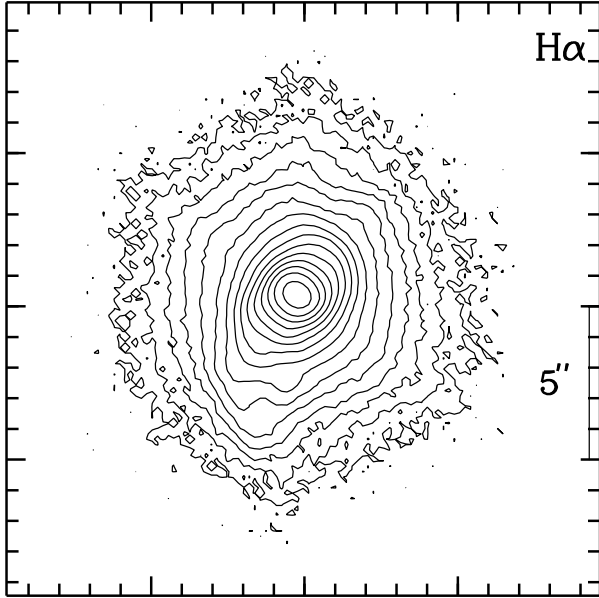
<sup>a</sup> Obtained from the long-slit [NII] spectra shown in Fig.9.

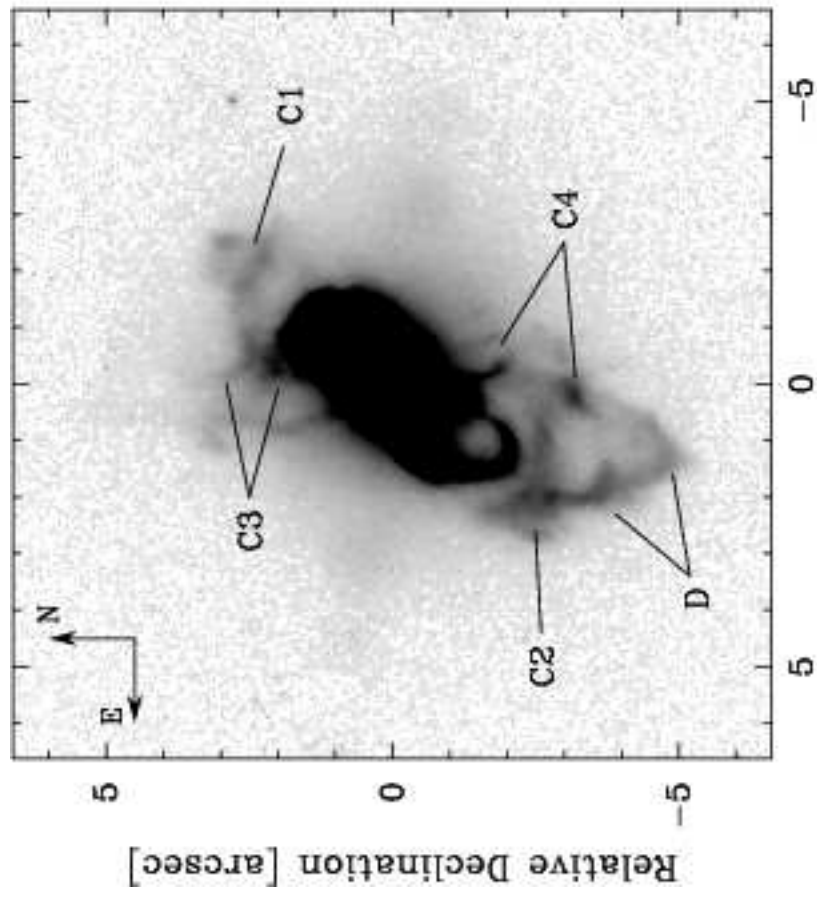
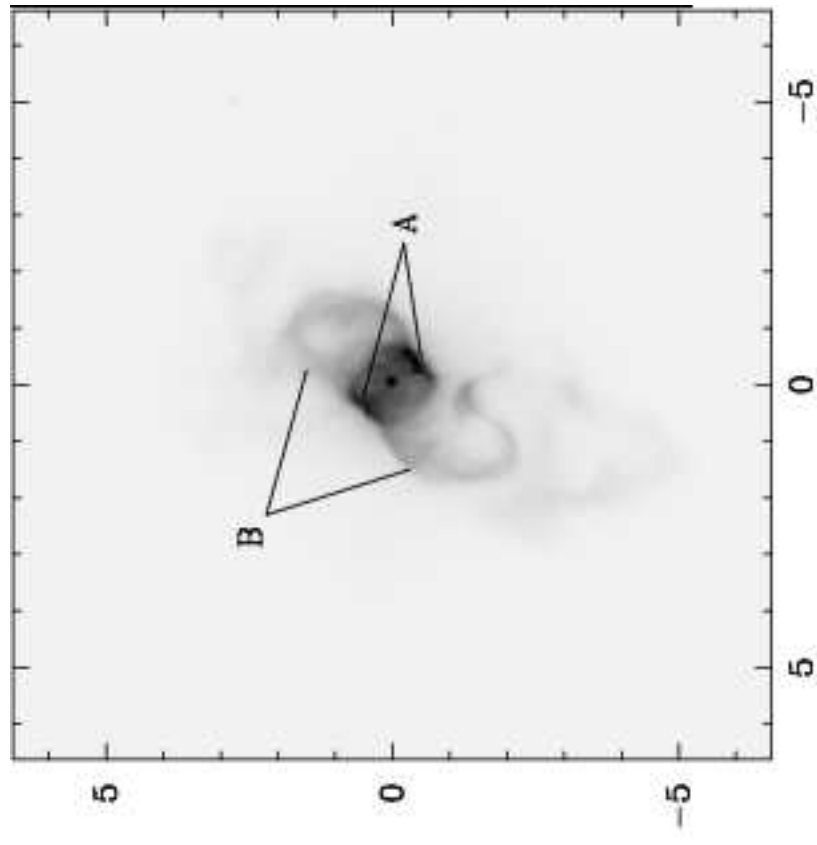
<sup>b</sup> Radial velocity with respect to the systemic velocity of the main nebular shell ( $V_{LSR} = 34.5$  km s<sup>-1</sup>).

<sup>c</sup> Angular distance from the central star along the corresponding PA.

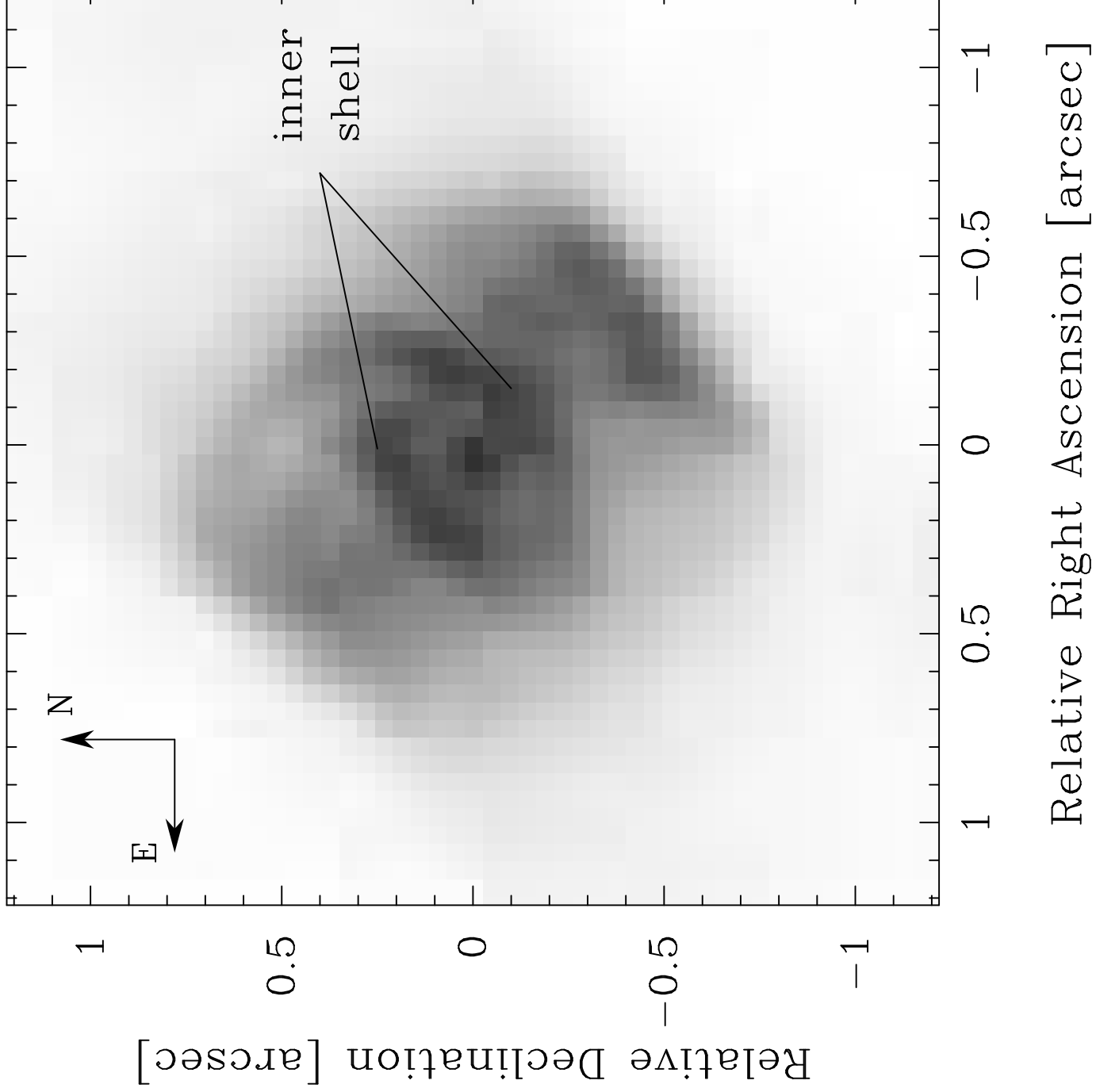
<sup>d</sup> Velocity width (FWHM) corrected of spectral resolution.

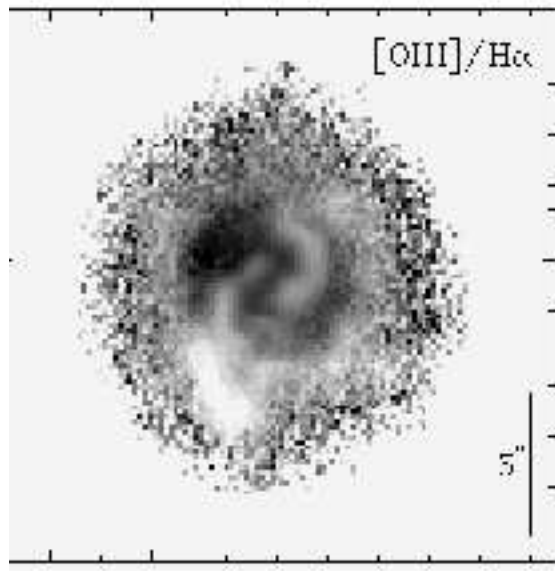
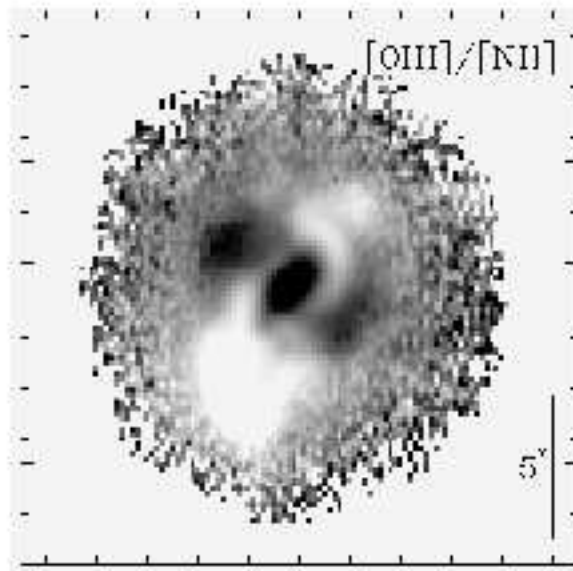
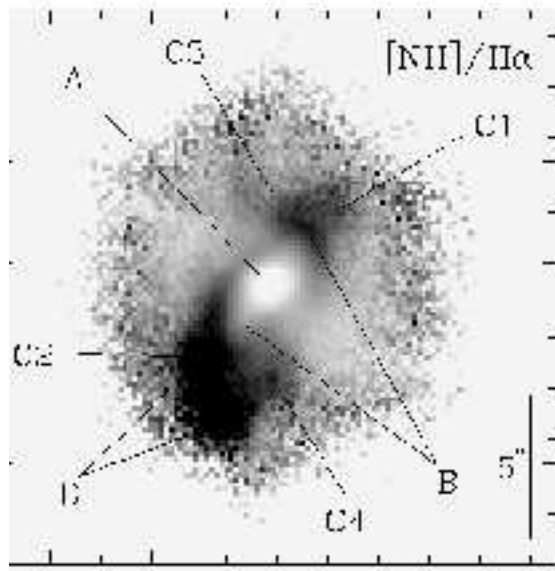
<sup>e</sup> Spatial extent (FWHM) corrected of spatial resolution.

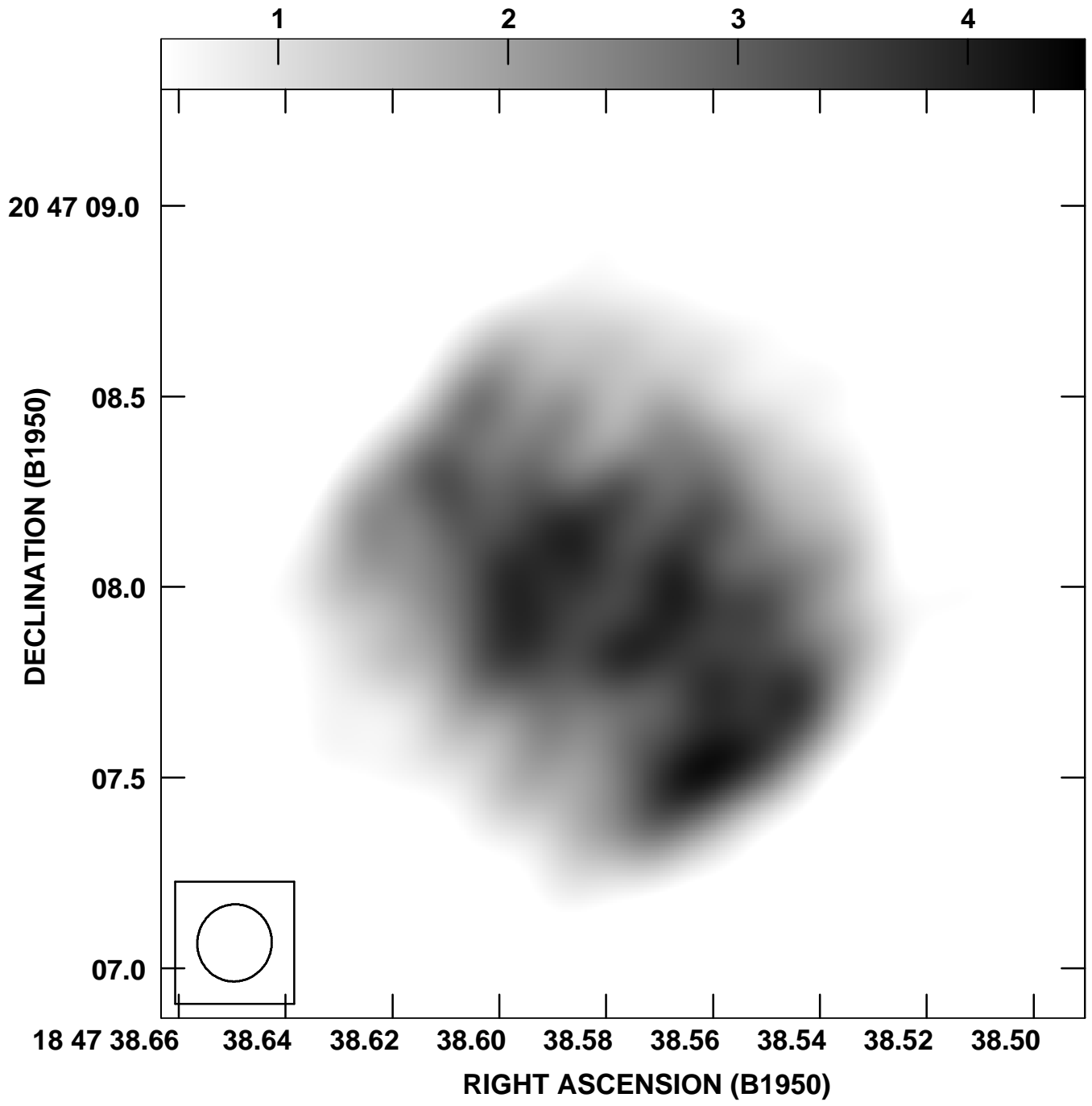


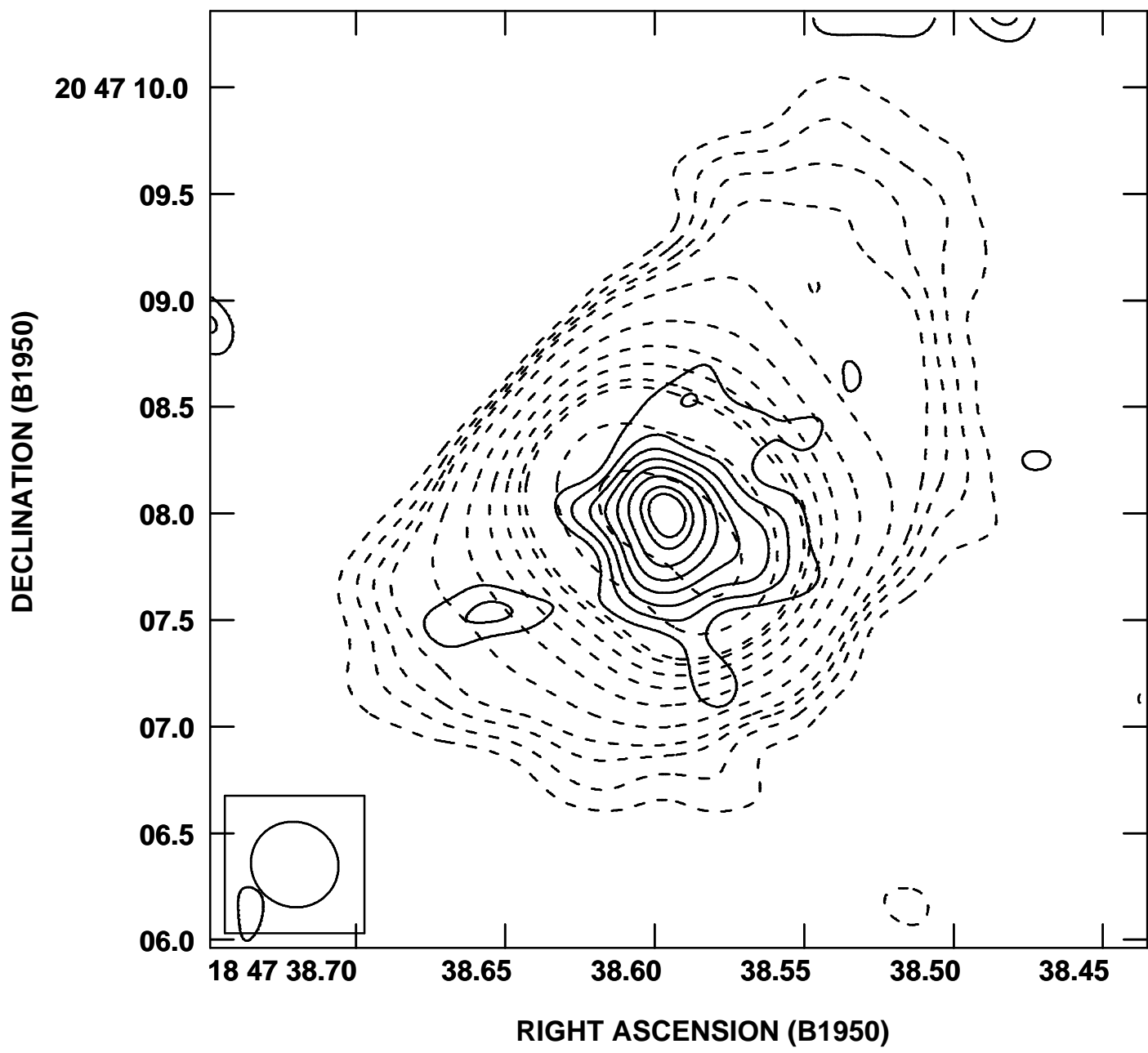


Relative Right Ascension [arcsec]

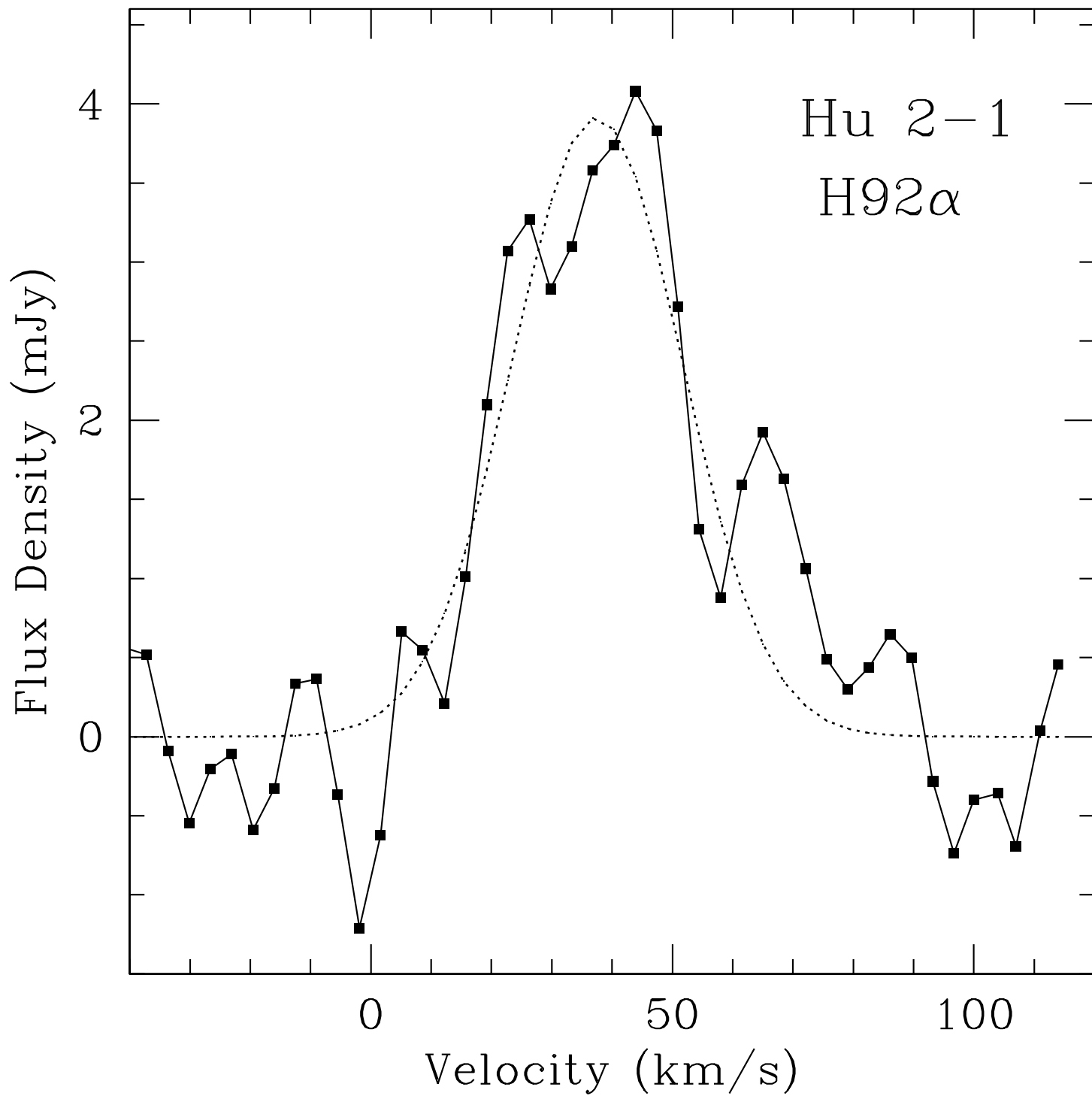


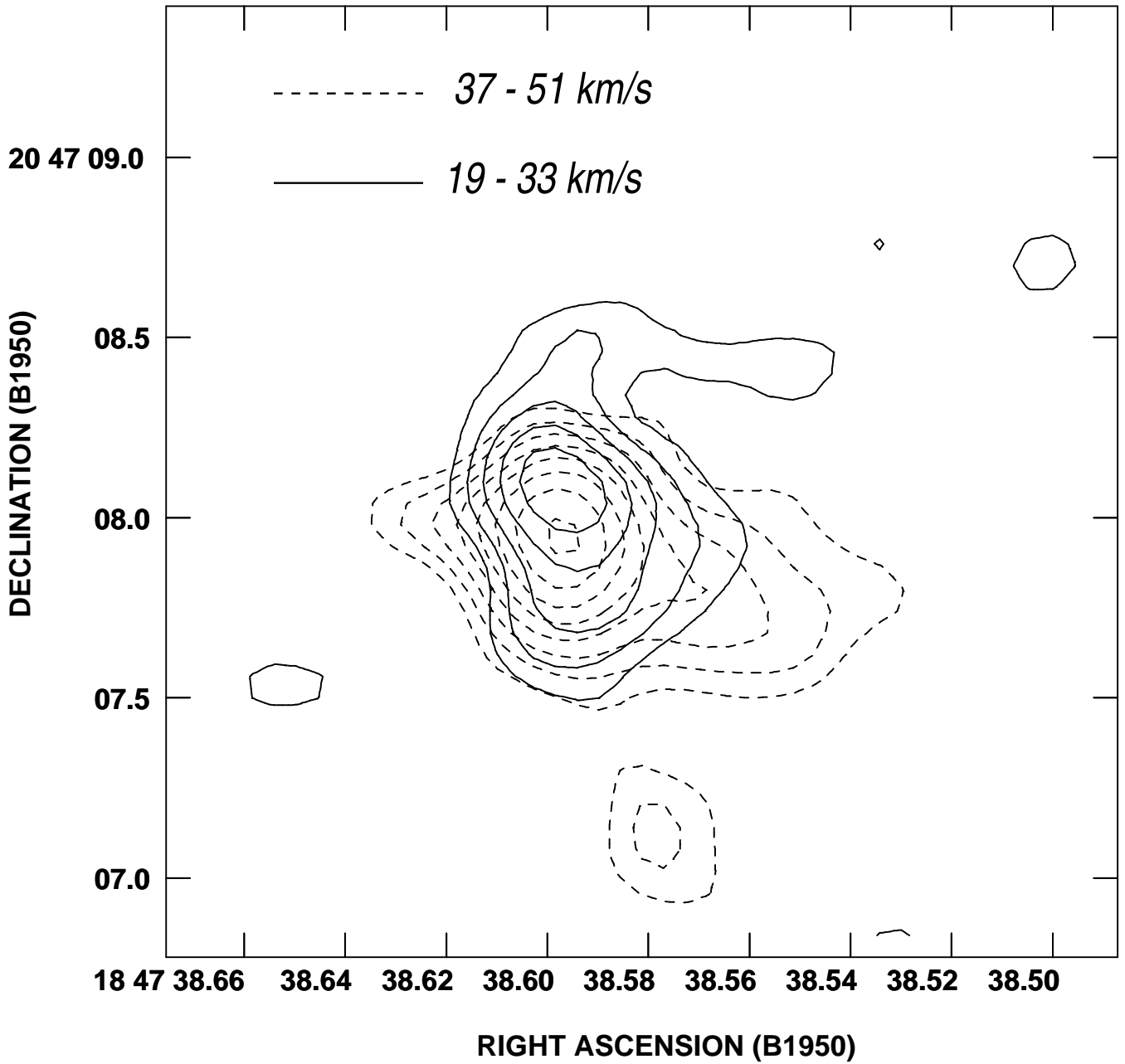




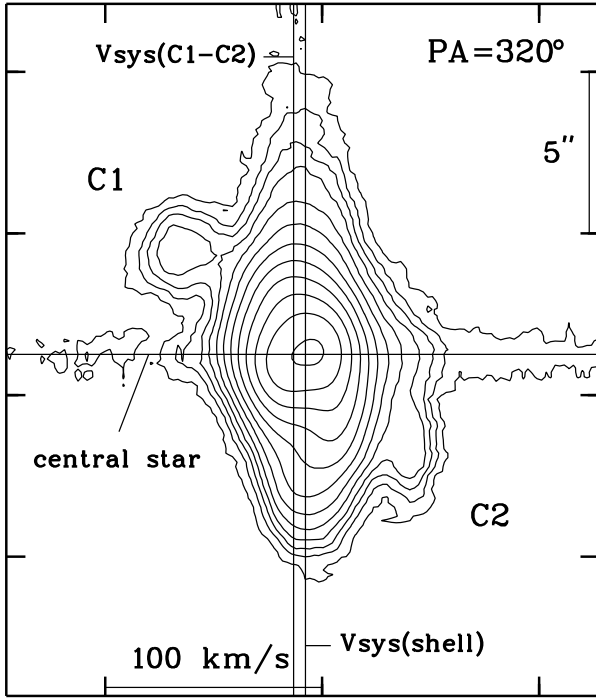




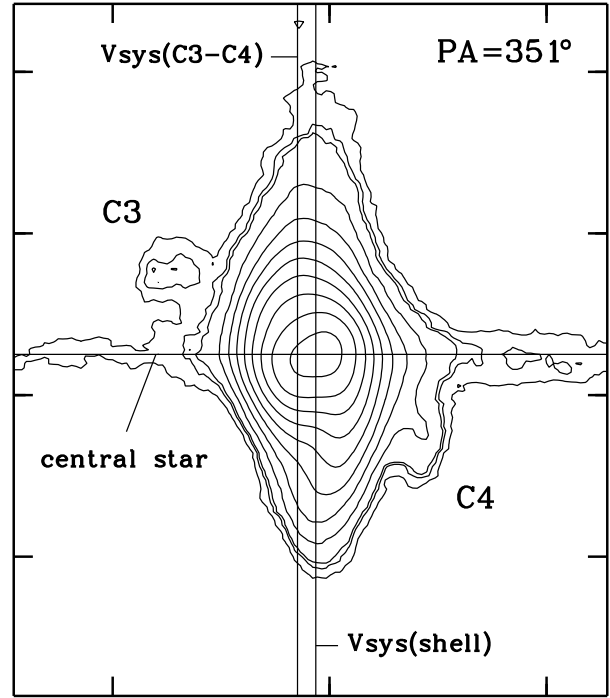




RELATIVE SPATIAL POSITION



RELATIVE RADIAL VELOCITY



RELATIVE RADIAL VELOCITY